Macromolecules

Article

pubs.acs.org/Macromolecules

Effects of Knots on Ring Polymers in Solvents of Varying Quality

Arturo Narros,*[,†] Angel J. Moreno,[‡,§] and Christos N. Likos[†]

[†]Faculty of Physics, University of Vienna, Boltzmanngasse 5, A- 1090 Vienna, Austria

[‡]Centro de Física de Materiales (CSIC, UPV/EHU) and Materials Physics Center MPC, Paseo Manuel de Lardizabal 5, E-20018, San Sebastián, Spain

[§]Donostia International Physics Center, Paseo Manuel de Lardizabal 4, E-20018 San Sebastián, Spain

ABSTRACT: We employ extensive computer simulations to investigate the conformations and the interactions of ring polymers under conditions of worsening solvent quality, in comparison with those for linear polymers. We determine the dependence of the Θ-temperature on knotedness by considering ring polymers of different topologies. We establish a clear decrease of the former upon changing the topology of the polymer from linear to an unknotted ring and a further decrease of the same upon introducing trefoil- or 5-fold knots but we find no difference in the Θ-point between the two knotted molecules. Our results are based on two independent methods: one considering the scaling of the gyration radius with molecular weight and one based on the dependence of the effective interaction on solvent quality. In addition, we calculate several shape-parameters of the polymers to characterize linear, unknotted, and knotted topologies in good solvents and in the proximity of the Θ-point. The shape parameters of the knotted molecules show an interesting crossover at a degree of polymerization that depends on the degree of knottedness of the molecule.

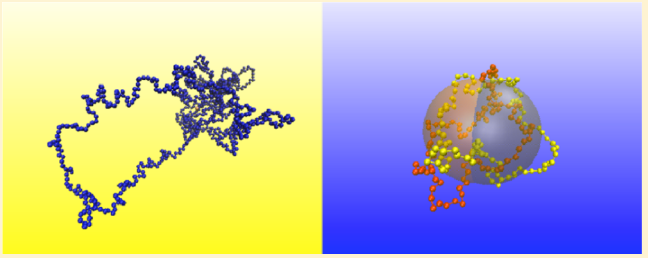

1. INTRODUCTION

In the context of polymer science, topology is ubiquitous when addressing issues related to the degree of knottedness of single looped molecules, i.e., of ring polymers, or with the entanglements between pairs of the same. The requirement of preserving the topological constraints is a crucial one, since long molecules have a high probability of being knotted.[1] A classical example is DNA, since it appears knotted in many biological systems such as cells or viral capsids.[2−4] Nature has developed special enzymes, the topoisomerases,[5] which alter the supercoiling of double-stranded DNA and appear to play a role in the replication and transcription in DNA chromosomes, although their unentangling mechanism is still not well-understood. The quantitative characterization of the topological state of ring polymers is carried out via the so-called *topological invariants*:[6,7] such are the Alexander and Jones polynomials[8] for single rings as well as the Gaussian linking number, m, for pairs of rings. When the latter assumes integer values $m \neq 0$, it signals a topologically entangled state between the rings. Computer simulation studies have increasingly focused on the investigations of the interplay between topology and physics in the context of ring polymer solutions. Typical issues examined are related to, e.g., the probability of knotting under various conditions,[9−11] the packing of knotted molecules,[4] scaling laws,[12−14] and knot localization,[15,16] as well as the impact of interchain and intrachain entanglements on the properties of ring polymer solutions.[17]

Experimentalists have also devoted, accordingly, considerable effort into the effects of topology as a factor to be quantified in their experiments. For example, electron microscopy allows us direct observation of the topology of molecules[18] and agarose-gel electrophoresis has been used to determine the topology of DNA experimentally.[19] Actually, in supramolecular chemistry, where molecules with identical bond sequence but different topologies have different physical properties, Nuclear Magnetic Resonance and X-ray crystallograpy allow us to characterize up to the 5-fold-knot.[20] Moreover, rheology applied to long, cyclic-polystyrene,[21,22] cyclic-polybutadienes,[23] and cyclic-polyelectrolites[24] shows striking results such as, for example, the reduction of the melt viscosity of ring polymers in comparison to that of linear chains by 1 order of magnitude. Additional experiments[21,22] show that addition of a small amount of linear chains in a ring melt increase the viscosity considerably, confirmed by fluoroscense microscopy.[25,26] This is a salient feature concerning with topological constraints and topology. From rheology and light scattering[27] experiments another striking effect has been found, which constitutes one of the central issues of this paper: the decrease of the Θ-temperature for solutions of ring polymers in comparison with those of linear chains.

The Θ-temperature of a polymer is defined as the temperature for which the statistics of a polymer is Gaussian, i.e., identical to that of an ideal chain. This state of affairs comes forward through an interplay between the ubiquitous steric repulsions between the monomers and the solvent-mediated attractions between the same, whose strength is temperature-dependent. At the Θ-point conditions, the second coefficient B_2 of the effective polymer−polymer pair potential vanishes. There are many works in the

Received: February 12, 2013
Revised: April 3, 2013
Published: April 16, 2013

   dx.doi.org/10.1021/ma400308x | *Macromolecules* 2013, 46, 3654−3668

literature,[28−33] in which the behavior of linear chains at or close to Θ-conditions are studied, e.g., the scaling laws determining the dependence of the gyration radius on the degree of polymerization N. Less is known about ring polymers, and in this case, work has focused exclusively on the trivial knot 0_1. In the first place, there is a crucial difference between linear and ring polymers of any fixed topology. In the former case, linear structure implies that triple- and higher-order contacts between the monomers can be ignored. As a result, linear chains at their Θ-point obey Gaussian statistics for all moments of their monomer distribution. There is no reason to expect the same to hold true for ring polymers: different moments might attain ideal behavior at different temperatures, therefore one has to define precisely what is meant by Θ-temperature of a ring. In what follows, we adopt two common definitions, one being related to the scaling of the gyration radius and one with the second virial coefficient of the effective ring−ring interaction potential. Here, the effective potential includes two contributions: one from the excluded-volume terms between the monomers and one from the topological constraint of no concatenation, the latter being known under the name *topological potential*.[34] Iwata and Kimura[35] as well as Tanaka[36,37] performed theoretical calculations of the topological part of the pair potential based in the Gaussian linking number, to predict location of the Θ-point for ring polymer solutions. Despite the good results and their agreement between simulations[38] and experiments,[39] the self-avoidance interaction has been included in these calculations in a rather crude, mean-field fashion. Work on the influence of molecular knottedness on the Θ-condition is rather limited,[40−43] thus the goal of this work is to address this issue. We have determined the location of the Θ-point of ring polymers in comparison to linear chains, differentiating the knottedness as a new ingredient that could influence its location. In addition, we have calculated the pair interaction potentials between two ring polymers under conditions of varying solvent quality, and compare them with those already calculated for linear chains.[32,44]

The quality of the solvent also incurs changes in the shapes of polymers. In good solvents, where repulsive interactions dominate, polymers are swollen. Below the Θ-temperature (poor solvents), the attractive part is stronger and the chains collapse into more compact objects, closer to spherical shape. Actually, due to the asymmetry of polymer chains in good solvent, a better shape representation of a polymer is an elongated ellipsoid than a sphere.[45] Quantitative measures of polymer morphology are the so-called *shape parameters*. They are sensitive to the symmetries of monomer distribution around the center of mass in regular volumes (spheres, cylinders or spheroids). They have been extensively used in the literature to characterize, e.g., linear and star polymer chains employing lattice simulations,[46−48] linear polypropylene with atomistic simulations,[49] and off-lattice simulations of linear chains.[50,51] Studies for linear and ring polymers of trivial topology (0_1-knots) and solvent quality distinction, showed a clear separation of the two types in terms of their shape parameters.[52,53] More recent works[54,55] have focused on the study of shape parameters and their dependence on knottedness, employing equilateral random polygons. It has been found that topology has a strong effect on the shape parameters. In this work, we undertake an extensive study of the latter by employing off-lattice simulations of a variety of ring polymers under different solvent conditions, comparing our findings with previous ones where appropriate. In what follows, we introduce the symbol τ to characterize the topology and we consider four topological classes of polymers: linear ones ($\tau = L$), unknotted rings ($\tau = 0_1$), as well as rings carrying a trefoil- ($\tau = 3_1$) and a 5-fold- ($\tau = 5_1$) knot.

The rest of the paper is organized as follows: In section 2, we expose in more detail the methods of techniques used in the literature to determine the Θ-point. In section 3, we define the investigated shape parameters. In section 4, we describe the model employed in our simulations and discuss the different sampling techniques applied. In sections 5 and 6, we show and discuss the results obtained for the Θ-point, employing, respectively, the scaling law of radius of gyration, R_g, and the calculation of effective pair potential, $V_{\text{eff}}(R)$. In section 7, we present our results for the shape parameters and for the four topologies considered in good- and Θ-like solvent conditions, whereas in section 8, we summarize and draw our conclusions.

2. METHODS OF Θ-POINT DETERMINATION

The Θ-point determination can be based either in the calculation of effective pair interaction between the centers of mass of two polymers, $V_{\text{eff}}(R)$, or by emplyoing scaling law predictions for the dependence of the radius of gyration R_g on the degree of polymerization N at the Θ temperature. In the former case, $V_{\text{eff}}(R)$ is defined as the constrained free energy of the two objects under the condition that their centers of mass are kept at separation R. The effective potential is thus, strictly speaking, a zero-density concept and its applicability in describing concentrated solutions can be limited to densities below the overlap concentration of the solution. This method has been employed for linear chains by several authors, applying both on-lattice[29,32,44] and off-lattice[30,33] simulations. It must be emphasized that the effective potential has a dependence on N, although it is expected that $V_{\text{eff}}(R)$ becomes a universal function of R/R_g at the limit $N \to \infty$; the form of this function depends both on solvent quality and on topology. The relation between $V_{\text{eff}}(R)$ and the second virial coefficient, $B_2(N)$, is given by:

$$B_2(N) = 2\pi \int_0^\infty \{1 - \exp[-\beta V_{\text{eff}}(R)]\} R^2 \, dR \tag{1}$$

where $\beta = 1/k_B T$, k_B being the Bolzmann constant and T the absolute temperature. The Boyle temperature, $T_B(N)$, is the temperature where $B_2(N)$ vanishes, and it exceeds the Θ-temperature T_Θ for finite values of N, approaching it from above at the limit of infinite length:[29,44]

$$\lim_{N\to\infty} T_B(N) = T_\Theta \tag{2}$$

A quantity related to the second virial coefficient $B_2(N)$ is the so-called stability integral, $I_2(N)$, employed by Krakoviack et al.,[44] which results by expanding the exponential term in eq 1 to linear order:

$$I_2(N) = 2\pi \int_0^\infty \beta V_{\text{eff}}(R) R^2 \, dR \tag{3}$$

Since $I_2(N)$ also depends on temperature through the dependence of $V_{\text{eff}}(R)$ on the latter, a new characteristic temperature $T_{\text{stab}}(N)$, at which $I_2(N) = 0$, can be defined. The stability temperature fulfills the inequality $T_{\text{stab}}(N) \leq T_B(N)$. Indeed this trivially follows from the inequality $\exp(-x) > 1 - x$ for every $x \neq 0$. However, the relation of the former temperature to T_Θ is not clear. For the linear polymer model employed by Krakoviack et al.,[44] it has been found that $T_\Theta < T_{\text{stab}}(N) < T_B(N)$. The same authors have employed the stability criterion as a necessary condition for the applicability of a description based on the effective pair potential, concluding that the latter offers a valid interaction to simulate polymer solutions only in the dilute and semidilute regimes.

The dependence of the effective potential $V_{\text{eff}}(R)$ on both topology and quality of the solvent has not been hitherto analyzed. Tanaka[36,37] and Iwata[35,39] have obtained approximate analytical expressions for the topological component $V_{\text{topo}}(R)$ of the effective potential $V_{\text{eff}}(R)$ of unknotted rings, based on the Gaussian linking number m and employing a mean-field approximation for the monomer distribution of the polymer. These results have been tested by simulations.[38] A lower Θ-temperature has been found for ring polymers than for their linear counterparts. The quantity $V_{\text{topo}}(R)$ has also been recently obtained in

dx.doi.org/10.1021/ma400308x | Macromolecules 2013, 46, 3654−3668

off-lattice simulations by Hirayama and co-workers[56] and on-lattice simulations by Bohn and Heermann[34] in good solvents. In the latter, the total effective potential $V_{\text{eff}}(R)$ has also been calculated for athermal solvents and unknotted rings, featuring a plateau-region at close distances, which is characteristic for ring polymers and has also been independently obtained in off-lattice simulations of the same.[57]

Another possibility to determine the Θ-temperature of a polymer is offered by the scaling of the gyration radius with the degree of polymerization, $R_g \propto N^x$, the exponent x assuming the value $x = \nu \cong 3/5$ in good solvents and $x = \nu_0 = 1/2$ in Θ-solvents.[28] Jang et al.[58] have applied this method together with force-field Molecular Dynamics to obtain a Θ-temperature for cyclic polyethylene (PE) that is 10% lower than linear-PE. This is consistent with experimental studies on polystyrene (PS), giving a lower value for cyclic-PS of 2% in comparison with its linear counterpart.[39] Knotted rings have not been considered in ref 58, however.

Unknotted ring polymers have a slightly different dependence of R_g on N than linear chains. It is well-established that self-avoiding rings with trivial topology, $\tau = 0_1$, have the same exponent $x = \nu \cong 3/5$ as linear chains, for sufficiently large values of N.[16,57,59−63] However, scaling arguments lead to a more specific prediction for infinitely thin unknotted rings:[59]

$$R_g(0_1) \cong \begin{cases} aN^{1/2}, & \text{if } N < N_{0_1}; \\ aN_{0_1}^{-\nu+1/2}N^{\nu}, & \text{if } N \gg N_{0_1} \end{cases} \tag{4}$$

where a is the bead size and N_{01} is the characteristic length of the unknot, which has a typical value $N_{01} \approx 300$.[11,64] The latter is related with the probability of observing a random polygon being unknotted.[9] eq 4 suggests a crossover from Gaussian behavior at small sizes to self-avoiding one at big sizes. This result, based on extensive simulations, suggests that a similar relationship might also hold for any set of infinitely thin rings with fixed knot type, but there is no exact result to confirm the validity of this assumption. A commonly used ad hoc-expression for the gyration radius of ring polymers has been proposed in ref14 and reads as follows:

$$R_g^{\,2}(\tau) = AN^{2\nu}[1 + BN^{-\Delta} + CN^{-1} + o(N^{-1})] \tag{5}$$

Here A, B, C, and ν are free parameters, which can in principle depend on the topology τ, whereas Δ is set to 0.5. Given the small sizes that we are going to consider in our work, we expect a small dependence on the type of knot; such a dependence is also noted in linear chains by Steinhauser.[28] eq 5 has been used by Dobay et al.[14] to calculate ν for the simplest topologies (0_1, ..., 8_x) and molecules consisting of up to $N = 600$ monomers.

The above considerations pertain to zero-excluded volume, non-phantom polymer rings. For real rings under conditions of varying solvent quality, Grosberg et al.[65] have put forward scaling considerations by employing the classical approach of Flory theory together with a weak topological invariant of the knots, called p-parameter, which describes the aspect ratio of a maximally inflated tube for a given knot type.[7] The following expressions have been derived regarding the dependence of R_g on temperature, molecular weight, and topology:[65]

$$R_g(\tau) \cong \begin{cases} aN^{3/5}\zeta^{1/5}p^{-4/15} & \text{in the good solvent regime, } \zeta > \sqrt{p/N}; \\ aN^{1/2}p^{-1/6} & \text{in the quasi-Gaussian regime, } |\zeta| < \sqrt{p/N}; \\ aN^{1/3}|\zeta|^{-1/3}\left[1 + |\zeta|^{-4/3}\left(\frac{p}{N}\right)^{2/3}\right] & \text{in the poor-solvent regime, } \zeta < -\sqrt{p/N}; \\ aN^{1/3} & \text{in the maximally tightened knot regime, } p \sim N, \end{cases} \tag{6}$$

Here $\zeta = (T_\Theta - T)/T_\Theta$ is the distance to the Θ-temperature. The validity of this equation has been later tested on a lattice model by Sun et al.,[66] obtaining good agreement.

According to eq 6 above, the molecule size at the Θ-temperature has a topological dependence. In particular, we expect the following relation to hold true:

$$\frac{\Delta R_g^{\,2}(\tau_1, \tau_2)}{N} \equiv \frac{R_g^{\,2}(\tau_1) - R_g^{\,2}(\tau_2)}{N} \cong p_1^{\,-1/3} - p_2^{\,-1/3} \tag{7}$$

where the radii of gyration $R_g(\tau_i)$, i = 1,2, are evaluated at the corresponding Θ-temperatures. The p-values for the topologies examined in this work are $p(0_1) = 1$, $p(3_1) = 16.33$ and $p(5_1) = 20.99$;[7] thus, we expect that $\Delta R_g^{\,2}(0_1,3_1)/N$ will be significantly larger than the quantity $\Delta R_g^{\,2}(3_1,5_1)/N$, as will be confirmed later.

3. DEFINITION OF SHAPE PARAMETERS

Here we define the shape parameters that we have employed to characterize the average form of ring polymers in varying solvent conditions. These are the relative shape anisotropy δ^*,[28,49,53] the prolateness S^*,[53] the asphericity b[28,49] and the acylindricity c.[28,49] They are defined with the help of the radius of gyration tensor:[49]

$$\mathbf{M} = \frac{1}{N}\sum_{i=0}^{N} \mathbf{s}_i \otimes \mathbf{s}_i \tag{8}$$

where $\mathbf{s}_i$ is the coordinate of the ith monomer with respect to the center of mass and ⊗ denotes the dyadic product. Diagonalization of the tensor $\mathbf{M}$ yields its eigenvalues λ_i, i = 1, 2, 3, which we order as $\lambda_1 \geq \lambda_2 \geq \lambda_3$. Out of these, we construct three invariants, I_i, i = 1, 2, 3, defined as

$$I_1 = \lambda_1 + \lambda_2 + \lambda_3 \tag{9}$$

$$I_2 = \lambda_1\lambda_2 + \lambda_2\lambda_3 + \lambda_3\lambda_1 \tag{10}$$

$$I_3 = \lambda_1\lambda_2\lambda_3 \tag{11}$$

Note that $I_1 = R_g^{\,2}$. Out of these, we define the aforementioned shape parameters as follows:

$$\delta^* = 1 - 3\langle I_2/I_1^{\,2}\rangle \tag{12}$$

$$S^* = \left\langle \frac{(3\lambda_1 - I_1)(3\lambda_2 - I_1)(3\lambda_3 - I_1)}{I_1^{\,3}} \right\rangle \tag{13}$$

$$b = \left\langle \lambda_1 - \frac{1}{2}(\lambda_2 + \lambda_3) \right\rangle \tag{14}$$

$$c = \langle \lambda_2 - \lambda_3 \rangle \tag{15}$$

where $\langle\cdots\rangle$ denotes an average over all configurations. Alternative definitions for the anisotropy and prolateness also used in the literature read as follows:[28,52,53,55]

$$\delta = 1 - 3\frac{\langle I_2 \rangle}{\langle I_1^2 \rangle} \tag{16}$$

dx.doi.org/10.1021/ma400308x | Macromolecules 2013, 46, 3654−3668

$$S = \frac{\langle (3\lambda_1 - I_1)(3\lambda_2 - I_1)(3\lambda_3 - I_1)\rangle}{\langle I_1^3\rangle} \quad (17)$$

The averages are carried out separately in the numerator and the denominator.

Both parameters $b \geq 0$ and $\delta^* \in [0,1]$ describe asphericity. They vanish for high symmetric configurations, such as tetrahedral or spherical, and are otherwise positive. For very long linear self-avoiding chains, we have $b/R_g^2 = 0.660$.[49] For the parameter δ^* some reference values obtained are, for example, $\delta^* = 0.3942$ for linear random walks (obtaned by $1/d$ expansion), as well as $\delta^* = 0.415$ and $\delta^* = 0.394$ employing renormalization group methods in good and Θ-solvents,[52] respectively. The parameter $S^* \in [-0.25,2]$ describes prolateness, assuming negative values for oblate and positive ones for prolate shapes. Some reference values of S^* are, for example, $S^* = 0.203$ for ring-shaped random walks[55] and $S^* \in [0.184,0.286]$ for stars with three or four arms.[53] Finally, the parameter $c \geq 0$ describes cylindrical symmetry, since $c = 0$ for cylindrical configurations.[28,49]

There has been considerable work dealing with the shape parameters for linear and star polymers,[28,46,48−52,67] much less that takes into account topological constraints,[53−55] and none in which the solvent quality dependence has been considered. We stress the recent work of Rawdon et al.,[55] in which a slightly different definition of asphericity and I_1 have been used, because of the "bias toward larger configurations" of these parameters, noted by Cannon and co-workers.[51] Rawdon et al. carried out a detailed analysis of asphericity and prolateness for different kinds of knots obtained by equilateral random polygons with up to $N = 500$ edges. They observed a common asymptotic value for the asphericity for polymers with a given knot, but the speed with which the asymptotic values is reached was found to decrease with the complexity of the knot. In addition, it was shown that less complex knots are less spherical than configurations of more complex knots.

4. MODEL AND SIMULATION DETAILS

4.1. The Model. Our simulations are based on an implicit solvent model,[28,68] in which the effects of the quality of the latter are modeled by an effective pairwise attraction between polymer beads. The model reproduces the effects of varying temperature and it is at the same time less computational expensive than other methods, such as solvent-accessible surface area (SASA)[69] or explicit solvent simulations. A drawback is that it can suffer from the existence of metastable configurations in which the system gets trapped,[69] therefore proper checks of the collected statistical data are mandatory.

The monomer−monomer interaction is modeled in the fashion employed by Huißmann et al.,[68] but with a Mie 24−6 potential[70] in place of the Lennard-Jones (Mie 12−6) one. The nonbonded monomer−monomer interactions are modeled by the potential $v_m(r)$ below, which includes a tunable parameter λ that allows for control of the depth of its attractive minimum:

$$v_m(r) = v_0(r) + \lambda v_{att}(r) \quad (19)$$

where

$$v_0(r) = \begin{cases} \infty, & \text{if } r \leq \sigma_h; \\ \dfrac{4 \times 2^{2/3}}{3}\varepsilon\left[\left(\dfrac{\sigma}{r}\right)^{24} - \left(\dfrac{\sigma}{r}\right)^{6} - \left(\dfrac{\sigma}{r_c}\right)^{24} + \left(\dfrac{\sigma}{r_c}\right)^{6}\right], & \text{if } \sigma_h < r \leq r_c; \\ 0, & \text{if } r > r_c \end{cases} \quad (20)$$

and

$$v_{att}(r) = \begin{cases} -\varepsilon, & \text{if } r \leq r_c; \\ \dfrac{4 \times 2^{2/3}}{3}\varepsilon\left[\left(\dfrac{\sigma}{r}\right)^{24} - \left(\dfrac{\sigma}{r}\right)^{6}\right], & \text{if } r > r_c \end{cases} \quad (21)$$

In the equations above, $r_c = 2^{1/9}\sigma$ is the minimum of the Mie 24−6 potential and σ_h is a hard core used to preserve the topology in our simulations, as it was done with previous models employed in Monte Carlo (MC) simulations.[57] Moreover, $\sigma = 1.2\sigma_h$ and in what follows the temperature T is always fixed at the value $k_B T = \varepsilon$. Accordingly, the effects of changing solvent quality are modeled by choosing different values of the parameter λ that scales the strength of the attractive potential $v_{att}(r)$. Whereas, for $\lambda = 0$, a purely repulsive monomer−monomer potential results, for $\lambda = 1$, the full Mie 24−6 interaction is at place; thus, an increase of λ corresponds to a worsening of solvent quality (i.e., in general to a lower temperature) in real experiments.

To speed up the calculations, we have further introduced a cutoff function $v_c(r)$[71] that multiplies $v_m(r)$ and reads as:

$$v_c(r) = \begin{cases} 1, & \text{if } r \leq r_1; \\ \dfrac{(r_2^2 - r^2)^2(r_2^2 + 2r^2 - 3r_1^2)}{(r_2 - r_1)^3}, & \text{if } r_1 < r \leq r_2; \\ 0, & \text{if } r > r_2 \end{cases} \quad (22)$$

This cutoff function smoothly bridges between the values $v_c(r_1) = 1$ and $v_c(r_2) = 0$ and it is thus suitable for producing continuous forces for a molecular dynamics (MD) simulation. We have chosen the values $r_1 = 1.5\sigma_h$ and $r_2 = 2\sigma_h$; see Figure 1. Finally, the

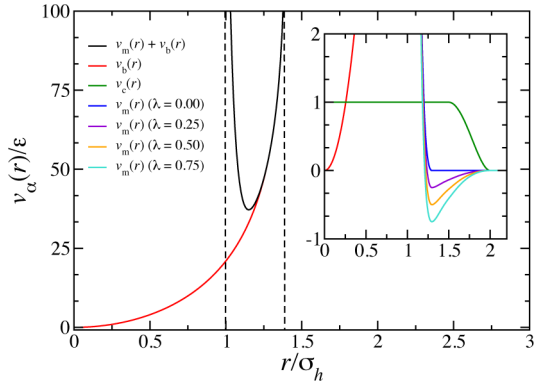

Figure 1. Various contributions $v_\alpha(r)$, $\alpha = m, b, c$, to the monomer−monomer potentials employed in this work, as described in the text. The inset shows a zoom of the potential $v_m(r)$ for various values of λ, as indicated in the legend, as well as the cutoff function $v_c(r)$.

dx.doi.org/10.1021/ma400308x | Macromolecules 2013, 46, 3654−3668

bonding between sequential monomers has been modeled by means of the standard finite-extensible nonlinear elastic (FENE) potential[72] $v_b(r)$

$$v_b(r) = \begin{cases} -\frac{1}{2}k\left(\frac{R_0}{\sigma_h}\right)^2 \ln\left[1-\left(\frac{r}{R_0}\right)^2\right], & \text{if } r \le R_0; \\ \infty, & \text{if } r > R_0 \end{cases} \quad (23)$$

with the values $k = 30.0\varepsilon$ and $R_0 = 1.4\sigma_h$. In Figure 1, we plot the various contributions to the total interaction potential for selected values of the parameter λ that scales the attractive part of the intermonomer interaction $v_m(r)$.

4.2. Simulation Details: Radius of Gyration. The ensemble configurations for the calculation of the gyration radius R_g were obtained by employing MD, MC, as well as Hybrid Monte Carlo (HMC)[73−75] simulations of a single molecule in different solvent conditions. Global movements of whole polymer sections were implemented as pivot- and/or crank-shaft moves[76,77] in MC and HMC simulations (PHMC). Note that in the case of ring polymers, crank-shaft and pivot modes must be checked to prevent topological changes, see Appendix A. Seven λ parameters have been used to model our solvent quality: λ = 0, 0.25, 0.50, 0.60, 0.70, and 0.75 for all systems and, additionally, λ = 0.65 for looped topologies. All the cases of solvent quality considered result into a minimum of the potential $v_m(r)$ smaller that k_BT in absolute value, reducing the probability of the aforementioned metastable states. Four topologies, the simplest ones, with five different number of monomers N = 100, 350, 500, 1000, and 1500 were considered to check the impact of topology on the Θ-point: linear ($\tau = L$), the trivial knot or unknot ($\tau = 0_1$), as well as the trefoil- ($\tau = 3_1$) and 5-fold ($\tau = 5_1$) knots. The starting configuration was generated from a self-avoiding random walk, in the case of linear chains, a circle for the unknot and analytical knot curves (torus knots) in the case of the 3_1 and 5_1 topologies.[7]

MC simulations where performed for the linear topology to generate an ensemble of about 10^5 configurations, separated by 10^4 MC steps. Every MC step was a combination of 100N single monomer movements and one pivot and crank-shaft movement, to improve our sampling and prevent trapping in metastable states. An initial equilibration time of 10^6 MC steps was performed before sampling. For linear chains there is no need to check for topology conservation, which makes the runs much faster than those for rings. In the latter case, given the higher correlation times for ring polymers and the risk of an expensive computation time for topology checking, we used MD simulation with Langevin thermostat[78] to generate the ensembles. A total of the order of 10^5 configurations were obtained, combining up to 10 independent MD simulations, after 10^6 MD steps of equilibration, with a sampling of 10^9 MD steps for each one. Longer sampling was performed for the biggest chain sizes (N = 1000 and N = 1500), extending to up to 10^{10} MD steps. We have stored data every 100N MD steps to prevent data that are either correlated or arise from metastable states. Multiple starting configurations, in a more detailed model of cyclic-polystyrene (c-PE), were also successfully employed in ref 58. Smooth profiles for the distribution $P(R_g^2)$ from independent MD runs were obtained in all cases. Figure 2 shows a typical case for a knotted topology ($\tau = 5_1$) close to Θ-conditions (λ = 0.70).

In addition, a second ensemble of around 10^5 configurations was also generated from 16 independent simulations for the most relevant cases (λ = 0.60,0.70) using the PHMC technique. Our HMC step was a combination of a short NVE simulation followed by a pivot and crank-shaft movement. We collected data every 10 steps during a total of 10^5 HMC steps. Such a procedure is useful in preventing a too correlated sampling, since the acceptance ratio lies slightly below 50%. Representative distributions for R_g^2 are shown in Figure 3. In Figure 3a, results for linear chains in good solvents, obtained with MC and PHMC simulations, are compared. The overlapping is good enough to be confident in our sampling. In Figure 3b, the same is shown the case of $\tau = 0_1$ topology, comparing the distributions obtained with MD and PHMC simulations close to the Θ-point. The overlapping is not as good as in the linear case, but the two distributions are sufficiently similar to one another.

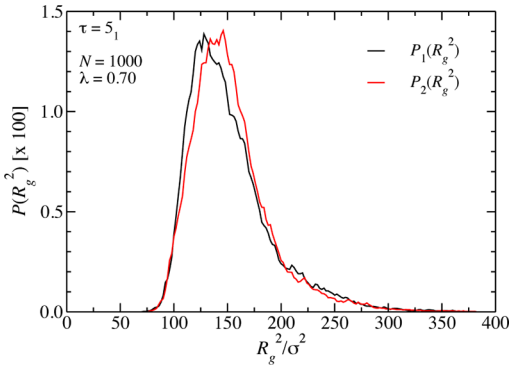

Figure 2. The distribution function $P(R_g^2)$ of the squared radius of gyration R_g^2 obtained by two independent runs, as explained in the main text, and for the case of $\tau = 5_1$-topology close to the Θ-point (λ = 0.70). The obtained expectation values for R_g^2 are $151.5\sigma^2$ (black line) and $152.8\sigma^2$ (red line). The results pertain to molecules with N = 1000 monomers.

4.3. Simulation Details: Effective Potential. We have calculated the effective pair interaction, $V_{eff}(R)$, between the center of mass (CM) of two molecules with 100 monomers for different solvent qualities and topologies, where R is the separation between the CM. The topologies studied are the same as those mentioned above and the solvent quality was varied by using the values λ = 0, 0.25, 0.5, and 0.75 in all the cases and, in addition, λ = 0.55, 0.6, and 0.7 for the linear chains and unknotted rings. In all cases, we have employed polymers consisting of N = 100 monomers, all of which interact by means of the same nonbonded potentials, both intra- and interchain ones. We employed MC simulations with the umbrella sampling technique,[57,79] to generate large ensembles (around 10^6 configurations) in every sampling window, using single monomer steps to collect data spaced every 10^4 monomer steps. The risk of metastable states[69] was reduced by using four different independent simulations with various starting configurations, to compare the obtained results and minimize the effects of such problems. Pivot and crank-shaft movements have not been used in this case, because they have a low acceptance probability for such small molecules at overlapping configurations.[44] In fact, ring polymers have a considerably smaller free volume than linear ones, so this problem would be more relevant for these topologies.

5. DEPENDENCE OF R_G ON SOLVENT QUALITY

A convenient way to quantify the dependence of R_g on solvent quality (i.e., on the λ-parameter) and to obtain a reliable first estimate of the location of the Θ-point λ_Θ is to plot the quantity R_g^2/N against λ for various values of N and for various values of

dx.doi.org/10.1021/ma400308x | Macromolecules 2013, 46, 3654−3668

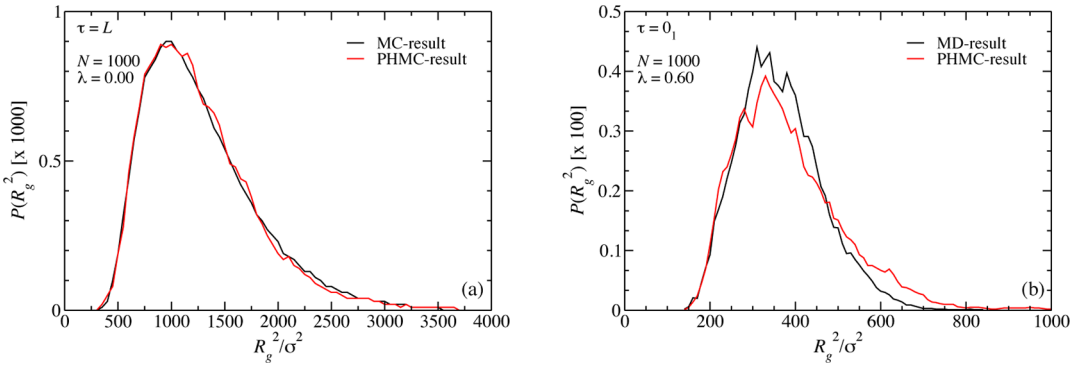

Figure 3. Same as Figure 2 but for (a) linear chains at good solvent conditions and (b) unknotted rings at Θ-like conditions, as indicated on the plots. The results in both cases were obtained for molecules consting of $N = 1000$ monomers. The legends display the different simulation techniques.

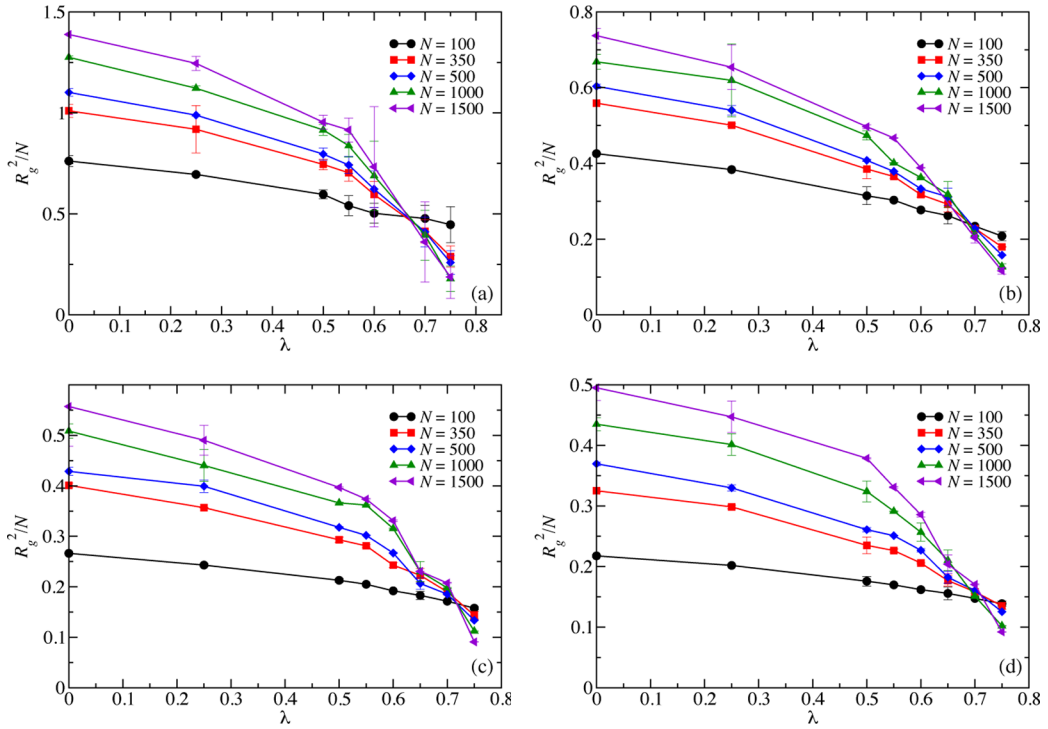

Figure 4. Plots of R_g^2/N against λ for the four different topologies investigated: (a) linear chain, $\tau = L$; (b) trivial knot, $\tau = 0_1$; (c) trefoil knot, $\tau = 3_1$; and (d) 5-fold knot, $\tau = 5_1$. The values of N considered are color coded as indicated in the legends. Error bars are in general as big as the symbol size; otherwise, they are explicitly shown.

λ.[28] In this way, and on the basis of eq 6, all the curves for a *fixed* topology should ideally cross at one common point, and the value of λ at that point could be identified with λ_Θ. The results of this procedure for the model at hand and for the four different topologies investigated in this work are shown in Figure 4. Within numerical uncertainties (note the error bars), the data sets at each panel seem to cross at a common point. According to the prediction of eq 6, the value of R_g^2/N at λ_Θ must scale as $R_g^2/N \cong p^{-1/3}$. For the trivial knot topology, Figure 4b, this value is considerably higher than those for the 3_1- and 5_1-topologies (Figure 4, parts c and d), the latter two being very similar. This finding provides an indirect confirmation of the ideas put forward by Grosberg et al.[65]

On the basis of the curves shown in Figure 4, we can make an estimate of the location of the parameter λ_Θ that corresponds to the Θ-temperature for each of the topologies considered. This is given by the λ-value at which the various curves cross. Since perfect crossing at a single point is not achieved for all curves, we focus on crossing for the highest N-values considered, for which we expect scaling-limit behavior to hold.[28] The obtained results are summarized on the second column of Table 1. It can be seen that we obtain $\lambda_\Theta(\tau = 0_1) > \lambda_\Theta(\tau = L)$, in agreement with previous predictions that the Θ-temperature of the ring topology is lower than that of the linear one.[58] It can also be seen that the Θ-temperature for the 3_1- and 5_1-topologies is predicted to be lower than that of the 0_1 topology but at the same time independent of the type of knot, i.e., $\lambda_\Theta(\tau = 3_1) = \lambda_\Theta(\tau = 5_1)$, an issue that demands further investigation.

To provide an independent check in determining the value λ_Θ we employ an alternative approach: instead of plotting R_g^2/N against λ, we determine an effective exponent $2\nu_\lambda - 1 \equiv x_\lambda$, by considering the quantity $R_g^2/N \sim N^{x_\lambda}$. At the Θ-point, one expects $\nu_{\lambda\Theta} = 1/2$ and thus $x_{\lambda\Theta} = 0$, meaning that the lines of R_g^2/N against N would be horizontal. The raw data are shown with points in Figure 5 along with fits that have been employed to determine the exponent ν_λ, and which we discuss in what follows.

dx.doi.org/10.1021/ma400308x | *Macromolecules* 2013, 46, 3654−3668

Table 1. Summary of the Findings Regarding the Location of the Θ-Temperature, Modeled by the Value λ_Θ, as Well as the Boyle and Stability Temperatures, Modeled by λ_B and λ_{stab}, Respectively[a]

τ	$\lambda_\Theta^{(a)}$	$\lambda_\Theta^{(b)}$	$\lambda_\Theta^{(c)}$	λ_B	λ_{stab}
L	0.66	0.65	0.64	0.62	0.63
0_1	0.68	0.68	0.68	0.67	0.70
3_1	0.72	0.71	0.68	–	–
5_1	0.72	0.71	0.68	–	–

[a]The first column describes the topology (τ) of the polymers, whereas the second, labeled $\lambda_\Theta^{(a)}$, shows the results obtained by considering the curves R_g^2/N versus λ (see Fig. 4). The third column, labeled $\lambda_\Theta^{(b)}$, describes the results obtained by fitting R_g vs. N with a simple power-law but dropping the data for the smallest value, $N = 100$. The fourth column, labeled $\lambda_\Theta^{(c)}$, shows the results obtained by fitting the curves R_g^2/N versus N according to eq 5 (see Figure 5) and locating the λ-value for which the exponent ν_λ has the value 1/2. The fifth and sixth columns show the values λ_B and λ_{stab} for which the second virial coefficient, $B_2(N)$, and the stability integral, $I_2(N)$, respectively, vanish. These results are based on simulations for the effective potential $V_{eff}(R)$ in section 6 and pertain to $N = 100$. Estimates for $\tau = 3_1$ and $\tau = 5_1$ were not possible in this case, due to the limited size of the rings (see text).

To begin with, it is evident by looking, e.g., at the resulting curves for $\lambda = 0.70$, that the $\tau = L$ and $\tau = 0_1$-topologies result into slightly negative slopes whereas those for the $\tau = 3_1$ and $\tau = 5_1$-topologies into positive ones. This is an unmistakable indication that for this value of λ the two former ones are below their Θ-points, whereas the two latter ones still slightly above. It is instructive to try to fit the points with power laws, because in this way some of the pitfalls associated with this procedure come to light. The most straightforward possibility is to fit the curves with a simple power law; these fits are shown in Figure 5 with dashed lines. The procedure works well for the linear topology, $\tau = L$, giving a scaling exponent $\nu = 0.601$ in good solvent conditions ($\lambda = 0$), close to the accurate result $\nu = 0.5876$.[80,81] For the ring topology the simple power-law fit also works well in the unknotted case, see Figure 5b. However, in the knotted topologies the quality of the power-law fits clearly worsens by decreasing the solvent quality; see Figure 5, parts c and d. The reason for this disagreement is that, as already alluded in eq 4, the simple power-law is an asymptotic property beyond some crossover value $N_\times$, which grows as the topology becomes more complicated. Our data include moderate N-values, which lie below the crossover ones, and their inclusion in the fits worsens the quality of the latter. If we drop the points related to the lowest N-value ($N = 100$), the simple power-law fits become much better (result not shown). The resulting values of ν lead to the Θ-points shown in the third column of Table 1 and they are essentially identical to those in the second column. This offers strong support to the finding that the Θ-point of knotted rings is lower than that of unknotted ones.

A more elaborate fitting procedure is given by employing eq 5, which has been previously used for ring polymers by other authors.[14,82] In all the fits we kept the exponent $\Delta = 0.5$ fixed, as suggested by Dobay et al.[14] For the remaining parameters in eq 5 we proceeded as follows. We obtained, for each topology τ, and in the limit of good solvent ($\lambda = 0$), the optimal values for the parameters A, B, C, and the exponent ν. Thereafter, the coefficients B and C were kept constant for all the subsequent values of λ, leaving only A and ν as free parameters. The reason for this choice is the physical anticipation that these two parameters capture the main effects that solvent has on the polymer size. We further note that we have not followed

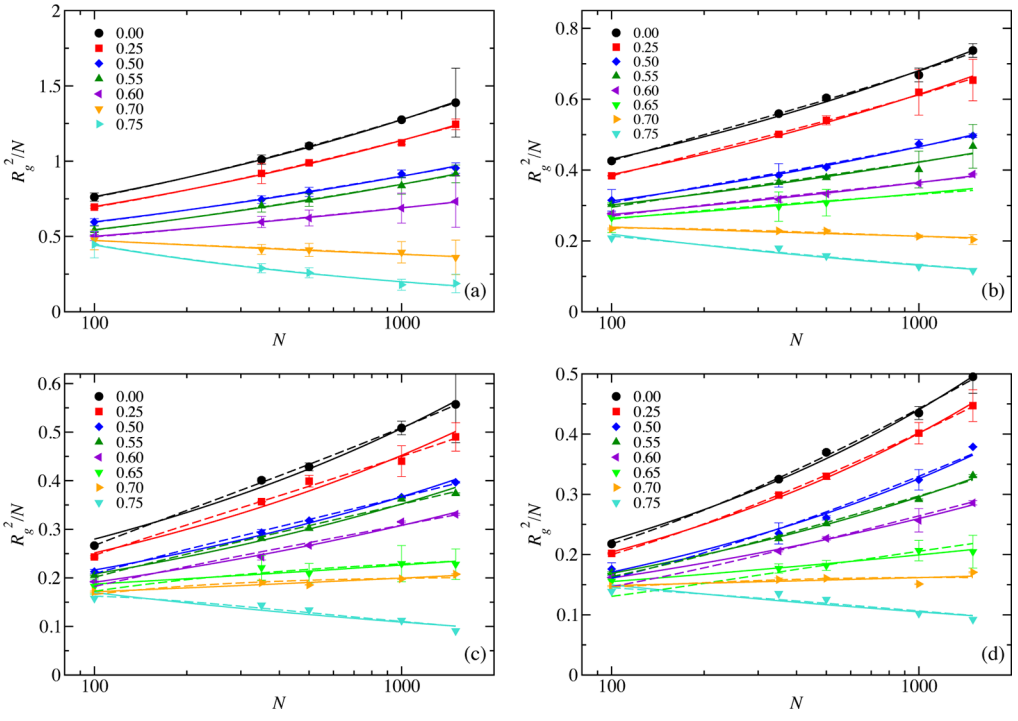

Figure 5. Plots of R_g^2/N against N for the four different topologies investigated: (a) linear chain, $\tau = L$; (b) trivial knot, $\tau = 0_1$; (c) trefoil knot, $\tau = 3_1$; and (d) 5-fold knot, $\tau = 5_1$. The values of λ, modeling the quality of the solvent, are color coded as indicated in the legends. Error bars are in general as big as the symbol size; otherwise, they are explicitly shown. Dashed lines correspond to fits to a simple power law, and continuous lines are fits according to eq 5.

dx.doi.org/10.1021/ma400308x | Macromolecules 2013, 46, 3654−3668

Orlandini's suggestion[82] to consider A independent of the topology in good solvent. Indeed, it was not possible to obtain reasonable fits by using this assumption.

The fits according to eq 5 are shown in Figure 5 with continuous lines. The resulting exponents ν_λ are shown in Figure 6 and the values of λ_Θ obtained by this procedure are summarized

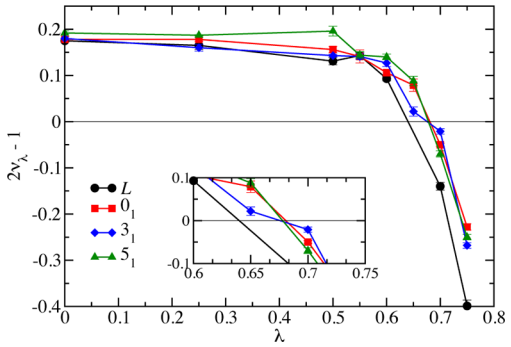

Figure 6. Effective exponent ν_λ as a function of λ obtained by the procedure of fitting the gyration radius data according to eq 5, as explained in the text. The four topologies are indicated in the legend. The inset shows a close-up of the curves in the neighborhood of the region $2\nu_\lambda - 1 = 0$, which serves for the determination of the corresponding Θ-points.

in the fourth column of Table 1. We confirm the previous results for the location of the Θ-temperature of the linear and trivial-knot rings. However, in contrast to the results in the second and third columns of Table 1, now we find no discrepancy between the λ_Θ-values for the three rings of different knotedness: within our accuracy, we obtain the result $\lambda_\Theta(\tau = 0_1) = \lambda_\Theta(\tau = 3_1) = \lambda_\Theta(\tau = 5_1)$.

The coincidence of the Θ-points of all ring polymers brought about by the last procedure above is an artifact of the fitting. First of all, the different slope of the R_g^2/N vs N curves for the unknotted rings as opposed to trefoil- and 5-fold-ones for $\lambda = 0.70$ (see Figure 5b–d above), clearly shows that they cannot share a common Θ-point. There is also additional, indirect evidence from previous work that the Θ-temperature depends on knotedness. First, Marcone et al.[62] have established that in three dimensions knots are fully delocalized below the Θ-point. If the knots were even weakly localized, meaning a knot length $l_K \sim N^t$ with $0 < t < 1$, then it would be plausible that in the $N \to \infty$-limit their effect would disappear since their length would become a vanishingly small fraction of the overall contour length. However, as the Θ-temperature is approached from below, the knots are spread out throughout the ring, causing thereby a substantial difference between knotted and unknotted rings, which should have an effect on the location of the Θ-point itself. Second, we refer to the work of Mansfield and Douglas.[83] Here, lattice polymers of various topologies have been simulated both in good solvents as well as at the exactly known Θ-point *of the linear chains* of the model. Plots of $R_g/N^{0.5}$ against N at the linear-chain Θ-point reveal a positive slope for all rings, a consequence of the fact that the rings' own Θ-temperatures are lower. At the same time, whereas the curves for the 0_1-topology are relatively flat, indicating a close proximity of $T_\Theta(\tau = 0_1)$ to $T_\Theta(\tau = L)$, those for the nontrivial knots have much more pronounced positive slopes, suggesting that their own T_Θ is inferior to that of the unknotted rings. We also note that Mansfield and Douglas found $\nu = 0.579$ for all knots at the Θ-conditions of the linear chains

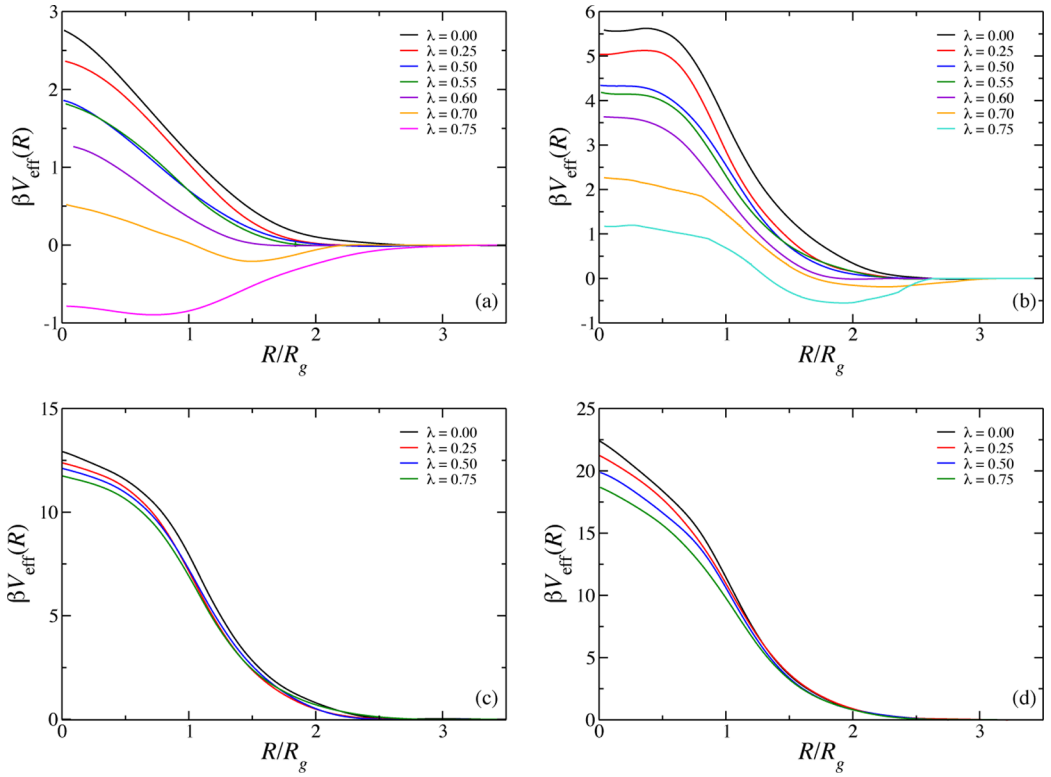

Figure 7. Effective center-of-mass potentials $V_{eff}(R)$ for the four topologies considered and for varying solvent quality: (a) linear chains, $\tau = L$; (b) trivial knots, $\tau = 0_1$; (c) trefoil knots, $\tau = 3_1$; (d) 5-fold knots, $\tau = 5_1$. The separation R between the centers of mass is scaled, at the horizontal axis, with the gyration radius of the individual molecule R_g at the given solvent conditions. The values of λ modeling solvent quality are indicated in the legends.

dx.doi.org/10.1021/ma400308x | *Macromolecules* 2013, 46, 3654–3668

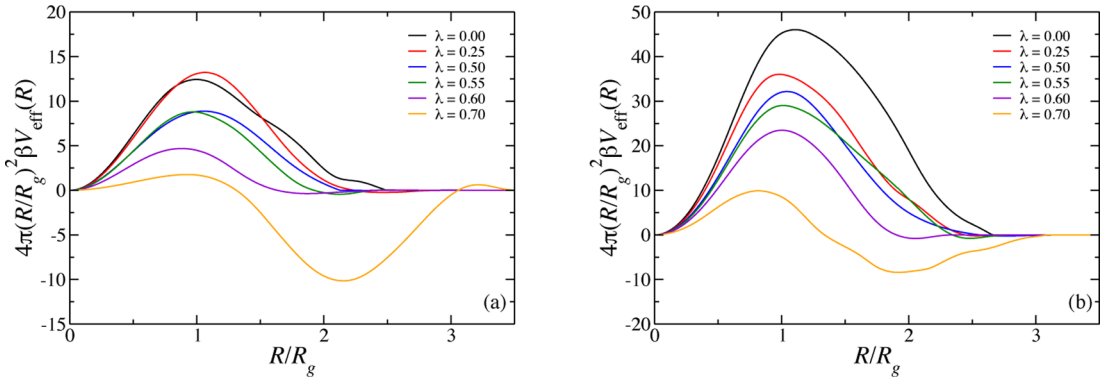

Figure 8. Integrand of the stability integral $I_2(N)$ of eq 3 for (a) linear chains and (b) ring polymers of 0_1-topology, scaled with the gyration radius R_g of the polymer at the corresponding solvent quality λ, as indicated in the legends. Results are shown for $N = 100$.

using eq 5, however the parameter Δ has been varied there as well, and points were weighted differently depending on the value of N.[83]

6. DEPENDENCE OF $V_{EFF}(R)$ ON SOLVENT QUALITY

Results for the center-of-mass effective potentials of the topologies considered and at the solvent qualities investigated are summarized in Figure 7. In all cases, we have employed polymers consisting of $N = 100$ monomers. We commence our discussion by considering the case of good solvents, $\lambda = 0$. For the linear polymer case, Figure 7a, we find the typical Gaussian shape of the effective interaction, thus confirming the universality of this shape for sufficiently long polymers, which has been previously observed in several investigations on lattice and off-lattice models.[44,57] This result is also in agreement with earlier theoretical results based on renormalization-group analysis.[84] The degree of polymerization $N = 100$ is apparently large enough for the linear topology, so that an effective interaction results which, when scaled on R/R_g, is independent of the underlying microscopic model employed. Similar conclusions can be reached for the effective potential between unknotted rings, Figure 7b. There it can be seen that the good-solvent effective potential features both a different shape than the one for the linear chains and a higher value at full overlap. This is a characteristic that brings forward the drastic effect of topology on the effective interaction. However, the shape of the $\lambda = 0$ effective interaction for $\tau = 0_1$ is practically indistinguishable from that obtained by means of different microscopic models both in the continuum[57] and on the lattice.[34] We can state, therefore, that $N = 100$ is sufficiently large for 0_1-rings, so that the scaling limit has been reached and $V_{eff}(R)$ attains a shape independent of the microscopic details, in agreement with previous findings.[57]

When the topology of the knotting becomes more complicated, the effective potential grows and the characteristic plateau at small separations, present in the $\tau = 0_1$-case, disappears. This can be seen in Figure 7c for the $\tau = 3_1$-topology and in Figure 7(d) for the $\tau = 5_1$-topology. The physical origin of this effect can be traced back to the fact that the knots cause an overall shrinking of the ring, as is readily visible in Figures 4 and 5. Accordingly, the steric hindrance for interpenetrating knotted rings is stronger than the one for their unknotted counterparts, the free energy cost growing with the complexity of the knot. This effect has been also seen in refs 57 and 85, in which a different microscopic model has been employed, in which the monomers of self-avoiding rings were modeled as tethered hard spheres. However, although the shapes of $V_{eff}(R)$ for the knotted topologies obtained in ref 57 are similar to the ones in the present work, the values obtained for the same are different. Contrary to the case of the linear- and 0_1-topologies, for the knotted topologies it appears that $N = 100$ is not a sufficiently high degree of polymerization to reach the scaling limit and the universal form in $V_{eff}(R)$ vs R/R_g, see also the discussion in ref 85.

Let us now proceed to the case of worsening solvent quality, $\lambda \neq 0$. For the linear case, we find a very good agreement with the previous results of Krakoviack et al.,[44] which is particularly satisfying in view of the fact that the results in ref 44 have been obtained within a completely different, lattice-based microscopic model. As the temperature is lowered (ref 44) or λ grows (this work), the strength of $V_{eff}(R)$ decreases. In the neighborhood of the Θ-point ($\beta_\Theta \cong 0.275$ in ref 44, $\lambda_\Theta \cong 0.65$ in this work), $V_{eff}(R)$ develops a shallow negative minimum at $R \cong 1.5R_g$ whereas it remains positive at full overlap, with $V_{eff}(R = 0)$ having a value of a fraction of k_BT. Finally, below the Θ-point, the strength of $V_{eff}(R)$ increases again, but turning fully negative. Still, it features a slightly repulsive bump at short distances in both the continuous model investigated here and in the lattice model of ref 44. Thus, even for worsening solvent qualities the behavior of the effective interactions of linear chains seems to be quasi-universal for a degree of polymerization as small as $N = 100$.

The evolution of the effective potential of unknotted ring polymers with varying solvent quality, shown in Figure 7b, is quite different from that of linear chains. Here, the negative part, which also starts appearing close to the Θ-point, remains localized in the region $R \cong 1.5R_g$; i.e., it does not penetrate into the small R-region even below the Θ-temperature. This is a manifestation of the fact that full ring overlap carries a much more substantial entropic cost than full overlap between linear chains. Indeed, as it was shown in ref 57, full overlap between two rings requires the squeezing of one inside the other, contrary to the case of linear chains for which topology does not place such a strict requirement. The negative parts that develop at the effective potential of unknotted rings nevertheless carry significant weight for the stability factor $I_2(N)$, since the integrand of the same involves a multiplication by R^2, see eq 3. The resulting integrands for linear and unknotted rings are shown in Figure 8.

For $\tau = 3_1$ and $\tau = 5_1$, the effect of worsening solvent quality is much less spectacular and it amounts solely to a reduction of the overall strength of $V_{eff}(R)$ without the appearance of any negative parts, see Figure 7, parts c and d. Knotted rings with $N = 100$ monomers are too small to display in their effective potential the typical negative parts that are associated with the reduction of the

dx.doi.org/10.1021/ma400308x | Macromolecules 2013, 46, 3654−3668

second virial coefficient and the appearance of an incipient Boyle-point (which, in turn, is a precursor of the Θ-point). In other words, the Boyle temperature for knotted rings of this particular size seems to be significantly farther away from their Θ-temperature—estimated previously on the basis of the scaling of R_g with N—than in the case of the unknotted counterparts. Simulations at even higher values of λ for the calculation of $V_{eff}(R)$ proved to be inefficient, since the knotted molecules become too tight there and the region of strong overlap cannot be sampled in a satisfactory way. Thus, we have refrained from attempting to obtain estimates of the Boyle-point λ_B of knotted rings with the present microscopic model.

On the basis of $V_{eff}(R)$, we can now calculate the second virial coefficient $B_2(N)$ and the stability integral $I_2(N)$ for linear chains and unknotted rings. Plots of these quantities against λ are shown in Figure 9. The points at which $B_2(N) = 0$ and $I_2(N) = 0$ are

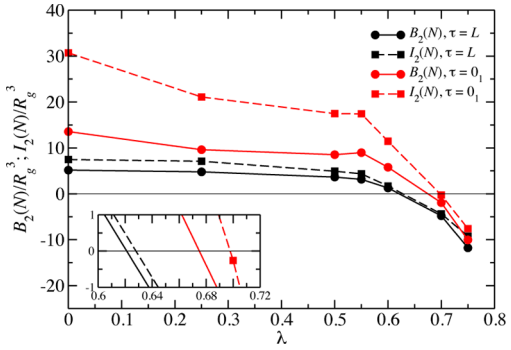

Figure 9. Second virial coefficient $B_2(N)$ (circles) and the stability integral $I_2(N)$ (squares) for linear chains ($\tau = L$) and ring polymers ($\tau = 0_1$), both of $N = 100$ monomers. See legend. Numerical results are plotted against the parameter λ, that models the solvent quality. The inset shows a zoom of the region in which these quantities vanish. Lines are guides for the eyes and connect the state points for which $V_{eff}(R)$ was obtained by simulation.

denoted as λ_B and λ_{stab}, respectively, and they are summarized in Table 1. For both cases $\tau = L$ and $\tau = 0_1$, the inequality $\lambda_{stab} > \lambda_B$ is obtained, consistently with the inequality $T_{stab} < T_B$.[44] From Table 1, we further see that the inequalities $\lambda_B < \lambda_{stab} < \lambda_\Theta$ hold for $\tau = L$, consistently with the finding $T_B > T_{stab} > T_\Theta$ found for the same topology by Krakoviack et al.[44] For $\tau = 0_1$, on the contrary, the inequalities read as $\lambda_B < \lambda_\Theta < \lambda_{stab}$. In other words, although $T_B > T_\Theta$ for finite N independently of topology, the ordering between T_Θ and T_{stab} is not unique and depends on τ (and, probably, on the microscopic model employed). Finally, comparing the Boyle points between two different topologies, we find $\lambda_B(\tau = 0_1) > \lambda_B(\tau = L)$. Interpreting the Boyle point as a finite-N precursor of the Θ-point ($N \to \infty$), this finding is consistent with the previous result that $\lambda_\Theta(\tau = 0_1) > \lambda_\Theta(\tau = L)$, i.e., with the fact that ring polymers have a lower Θ-temperature than chemically identical linear ones.

7. SOLVENT QUALITY AND SHAPE PARAMETERS

The values of the shape parameters introduced in section 3 are plotted in Figure 10 for all the topologies considered and for the case of good solvent ($\lambda = 0$). The corresponding results for the case of Θ-like solvent ($\lambda = 0.70$) are shown in Figure 11. For comparison, in Table 2, we summarize values previously determined in the literature. At the same time, we include there the values of the shape parameters obtained in this work by extrapolation to $N \to \infty$. The latter are obtained by plotting the simulation values against $1/N$ as shown exemplarily in Figure 10, parts e and f, fitting the data by a straight line and taking the extrapolation to $1/N \to 0$. We note that in this fit each point has been assigned a weight equal to $1 - E$, where E is the relative error bar.

The asphericities δ^* and b/R_g^2 in good solvent are shown in Figure 10, parts a and b. Both measures of the asphericity show similar behavior. There is a "gap", at all N-values, separating the data of the linear chains from those of the three topologically distinct rings. The results reveal that the rings are more spherical than their linear counterparts. For low N-values, $N \lesssim 500$, the asphericities of the knotted rings are also clearly separated from those of the unknotted ones. The trefoil and 5-fold rings are considerably more spherical in shape than the 0_1-rings. This feature can be understood by the fact that, in small rings, knots are relatively tight and thus they contribute to suppress fluctuations that strongly deviate from the spherical shape. On the other hand, as N grows, the values of the asphericity seem to converge to a common point for all rings. This feature was also reported by Rawdon et al.,[55] who used the parameter δ of eq 16 instead of the parameter δ^* used here. Our data also show an interesting "inflection region" of the δ^*- and b-parameters for the 3_1- and 5_1-rings around $N \in [350, 400]$. A similar feature is also observed for the prolateness parameter S^* in Figure 10c. Such a change in slope was not found in the work of Rawdon et al.,[55] but they employed a model of random equilateral polygons instead. It is tempting to associate this behavior with a characteristic crossover $N_\times$ from Gaussian to self-avoiding behavior put forward in eq 6, according to which $N_\times \sim p$. In ref 55, a crossover in the asphericity of 0_1-rings, for which $p = 1$, is seen for $N_\times \cong 25$. Given that for 3_1- and 5_1-rings $p \cong 20$, it is plausible that for these topologies $N_\times \cong 500$, i.e., in the region in which we observe the crossover for the shape parameters.

The parameters δ and δ^* have been used much more often in the literature to describe asphericity than b/R_g^2. Combining all the literature values for the δ^*-paremeter of the linear chains in good solvents summarized in Table 2, we obtain an average value $\delta^* = 0.429$, differing from our result $\delta^* = 0.434$ by 1%. Regarding the parameter b, in Table 2 we quote the only two values of the latter available for linear chains: $b/R_g^2 = 0.659$[28] and $b/R_g^2 = 0.660$,[49] smaller than our extrapolated value ($N \to \infty$) of $b/R_g^2 = 0.672$ by about 2%.

According to theory,[52,86] the δ^*-values for ring polymers in good solvent lie around $\delta^* \cong 0.260$, see Table 2. However, most of the values for ring polymers reported are for the δ parameter, eq 16, which is slightly larger than δ^*. In addition, in many works no differentiation has been made between knotted and unknotted rings; see the entries carrying superscript [c] in Table 2. Our value $\delta^* = 0.247$ obtained for $\tau = 0_1$ is lower by about 4% than previous values. The values of δ^* decrease with knot complexity, which is reasonable since the addition of knots renders the molecule more tight and thus more spherical. According to the findings of Marcone et al.,[62] the knots at good solvent conditions are weakly localized, so that at the $N \to \infty$-limit they occupy a negligibly small fraction of the rings; thus, all asphericities should converge to a common value. However, the sizes N used here are still too small to enable us to check this conjecture.

The prolateness parameter S^* is shown in Figure 10c. All polymers are prolate in shape ($S^* > 0$) and, as expected, the linear chains are the most prolate ones, and their S^*-values are separated from the rings by a gap. This prolate shape for *flexible* rings should be contrasted to the typical oblate shapes obtained

dx.doi.org/10.1021/ma400308x | Macromolecules 2013, 46, 3654−3668

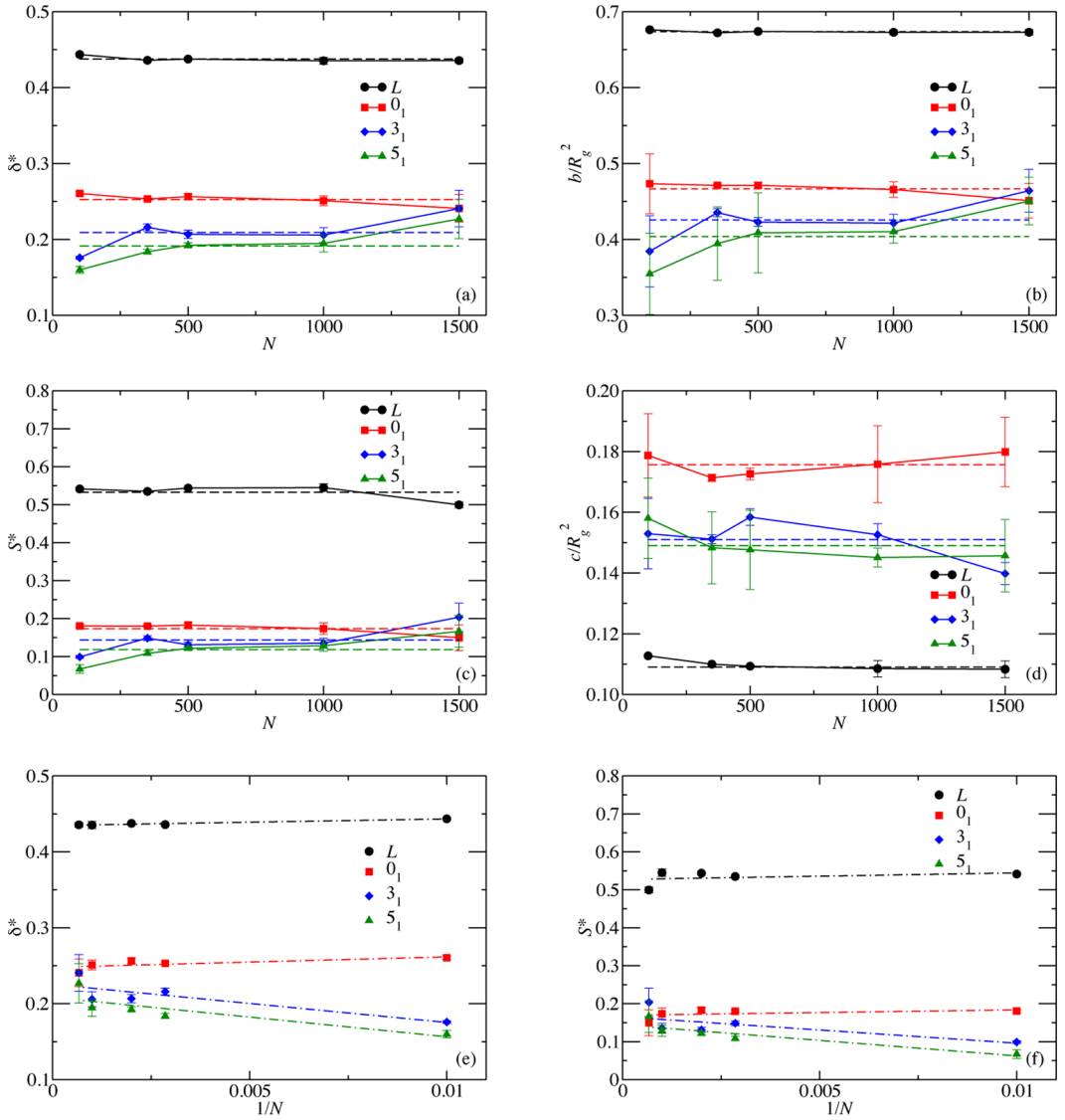

Figure 10. Dependence of the shape parameters for the four topologies considered, as indicated in the legend, and for good solvent quality, $\lambda = 0$, on the degree of polymerization N. Key: (a) the asphericity parameter δ^*; (b) the alternative asphericity paremeter b/R_g^2; (c) the prolateness parameter S^*; (d) the acylindricity parameter c/R_g^2. The solid lines are guides for the eyes. The dashed lines indicate the averages over all the N-values for each case. In panels e and f, we show the parameters δ^* and S^*, respectively, plotted against $1/N$. Here, the dash-dotted lines show the best fits through the points. Extrapolation of the values to $1/N \to 0$ yields the entries quoted in Table 2.

for small rings with stiffness, see ref 63. In analogy with the trends observed for the asphericity, we find that the knotted rings are the least prolate ones (smallest values of S^*) at the smallest values of N. However, for large N all rings seem to converge to a common value.[55] The inflection region around $N \in [350,400]$ for knotted molecules observed in the asphericity parameters is present for S^* as well. The consistency of our results with previously published ones can be seen in Table 2. Our extrapolated value $S^* = 0.527$ for linear chains in good solvents lies within 3% of the value $S^* \cong 0.540$ from most of previous simulations. For $=0_1$-rings, our value $S^* = 0.169$ is considerably different (by more than 10%) from the one in ref 53 obtained from lattice simulations.

The acylindricity parameter c/R_g^2 is shown in Figure 10d. Evidently, the linear chain has the most cylindrical shape of all polymers considered, a feature consistent with its pronounced asphericity and prolateness discussed before. The two knotted rings have a smaller value of c than the trivial knot, which seems counterintuitive at first sight. Since knotted topologies result into more spherical shapes than unknotted ones, one might expect that the knotted rings should also be less cylindrical. However, we have to keep in mind that the parameter c only measures the difference between the two smallest values of the gyration tensor; i.e., it is independent of the largest eigenvalue. For knotted rings, which fluctuate less than the unknotted ones, the two smaller eigenvalues lie closer to each other than in the case of the 0_1-rings, thus leading to a lower acylindricity parameter. Regarding comparisons with previous results, we only found one data point for linear chains, ref 49, and the value there, $c/R_g^2 = 0.110$, is in agreement with the result of our work, $c/R_g^2 = 0.108$; see Table 2. Acylindricity parameters for ring polymers have not been calculated before, to the best of our knowledge.

In Figure 11, the shape parameters for Θ-like solvent conditions, $\lambda = 0.70$, are shown. We emphasize that this common value $\lambda = 0.70$ has been chosen just for comparison between results for the different topologies. Actually, $\lambda = 0.70$ is

dx.doi.org/10.1021/ma400308x | Macromolecules 2013, 46, 3654−3668

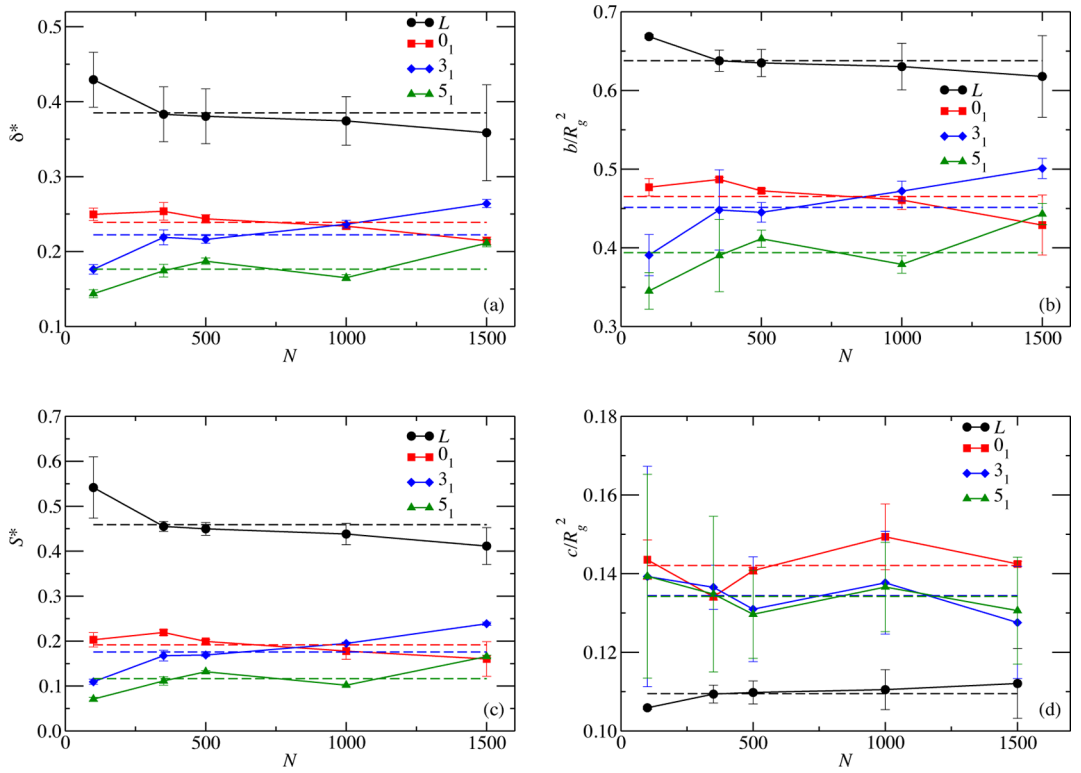

Figure 11. Same as Figure 10, panels a–d, but for a Θ-like solvent quality, $\lambda = 0.70$.

Table 2. Summary of the Values of the Shape Parameters for Linear ($\tau = L$), Ring ($\tau = 0_1$), Trefoil ($\tau = 3_1$), and 5-Fold Knot ($\tau = 5_1$) Topologies in Good Solvents (This Work: $\lambda = 0$) and Θ-Like Solvents (This Work: $\lambda = 0.7$)[a]

		good solvent				Θ-like solvent			
τ	obtained by	δ^*	b/R_g^2	S^*	c/R_g^2	δ^*	b/R_g^2	S^*	c/R_g^2
L	theory[86]					0.377			
	theory[52]	0.415				0.394		0.475	
	off-lattice[28] ($N \leq 2000$)	0.434	0.659			0.394	0.625		
	off-lattice[50] ($N \leq 250$)	0.429				0.397	0.625		
	off-lattice[51]	0.447		0.572					
	lattice[52] ($N \leq 220$)	0.431		0.541		0.396			
	RIS-PP[b,49] ($N = 751$)	0.410	0.660		0.110				
	lattice[53] ($N \leq 8192$)	0.430		0.539					
	lattice[48] ($N \leq 1000$)	0.433		0.544		0.389		0.465	
	this work	0.434	0.672	0.527	0.108	0.362	0.618	0.418	0.111
0_1	theory[c,86]					0.261			
	theory[c,52]	0.260				0.246			
	lattice[c,52] ($N \leq 220$)	0.262							
	lattice[c,d,53] ($N \leq 8192$)	0.255		0.191					
	ERP[d,e,55] ($N \leq 500$)	0.255				0.246			
	this work	0.247	0.462	0.169	0.174	0.231	0.456	0.184	0.142
3_1	ERP[d,e,55] ($N \leq 500$)	0.256							
	this work	0.225	0.446	0.165	0.149	0.247	0.479	0.212	0.131
5_1	ERP[d,e,55] ($N \leq 500$)	0.263							
	this work	0.208	0.430	0.144	0.144	0.192	0.416	0.139	0.131

[a]The fitting error bars typically lie between ±0.001 and ±0.01. In some cases, we indicate explicitly the value N of the longest polymer considered. [b]RIS-PP: rotational-isomeric-state for polypropylene. [c]Results from a combination of knotted and unknotted topologies. [d]A slightly different definition of the value δ^* has been employed, namely the parameter δ shown in eq 16 in section 2. See the original references for details. [e]ERP: equilateral random polygons.

slightly higher than most of the λ_Θ-values shown in Table 1; therefore, comparisons with shape-parameter values in the literature obtained at the Θ-point must be made with due care.

Comparison of the curves in Figure 11 and Figure 10 reveals similar trends in both good and Θ-like solvent conditions. Still, some interesting differences are found. First, the gaps between

dx.doi.org/10.1021/ma400308x | Macromolecules 2013, 46, 3654−3668

the different topologies are still present but they close up. This is a consequence of the fact that the presence of monomer−monomer attractions drives the polymers toward more spherical shapes. Second, the data points show bigger error bars in comparison to their good-solvent counterparts, as a manifestation of the strong fluctuations of the molecules due to the vicinity of a Θ-point, at which a tricritical singularity takes place at the thermodynamic limit.[44]

For the asphericity parameters, in Figure 11, parts a and b, a trend toward convergence to a common value for increasing N can be discerned again, as pointed out also by Rawdon et al.,[55] but the fluctuations are much stronger than in good solvent conditions to allow for safe conclusions. The value of δ^* in Θ-conditions reported for linear polymers is around $\delta^* = 0.390$, see Table 2. Our value $\delta^* = 0.362$ is somewhat lower, mainly due to the fact that the selected value $\lambda = 0.70 \gtrsim \lambda_\Theta$ (see Table 1) corresponds to solvent conditions slightly worse than at the Θ-temperature. However, regarding our value $b/R_g^2 = 0.618$ for linear chains in Θ-solvent, we do find a very good agreement with the value 0.625 found by Steinhauser.[28]

Theoretical predictions for ring polymers in Θ-solvent, without distinction of the knotedness,[52] provide a value $\delta^* = 0.246$. Simulations of 0_1-equilateral random polygons yield the same value 0.246 for the closely related parameter δ.[55] Our value for 0_1-rings is $\delta^* = 0.231$, again lower than the ones found in the literature, and again probably due to the slightly poorer solvent conditions described by the selected $\lambda = 0.70$.

Regarding the prolateness parameter S^* at Θ-conditions, shown in Figure 11c, a trend can be observed by which the linear chains become less prolate as N increases, matching the simultaneous trend of becoming more spherical, observed in Figure 11, parts a and b. Our value, $S^* = 0.418$, for the linear topology is again lower, by roughly 10%, than previously quoted ones, which were calculated by means of lattice simulations[48,53] exactly at the Θ-point. Finally, the acylindricity parameters, shown in Figure 11d, maintain the trends observed for good solvent conditions, though they feature a clear reduction of their values for the ring topologies.

8. CONCLUSIONS

We have presented a detailed analysis of the dependence of conformations, (sizes and shapes) or knotted and unknotted rings polymers on solvent quality, the latter having been modeled by a tunable effective attraction between the monomers in an implicit solvent model. To this end, we have applied a variety of efficient sampling techniques, such as MC, MD and HMC simulations, combining local and collective moves and introducing an algorithm to ascertain the conservation of topology for the latter. The results for three different rings topologies, trivial knots, trefoil knots, and 5-fold knots have been compared with one another as well as with those from linear polymers, which provide a point of reference.

Detailed analysis of the scaling behavior of the gyration radius R_g with the degree of polymerization has led to the determination of the Θ-temperatures of rings. We have shown that a straightforward application of a power-law dependence is problematic, at it tends to be contaminated by data at low-values of N. This issue is particularly important for knotted rings, since the characteristic value $N_\times$ at which a crossover to swollen behavior is observed grows with the complexity of the knot. On the basis of our analysis, we have confirmed that the Θ-temperature of unknotted rings is lower than that of their linear counterparts. For knotted rings, our results show a further decrease of T_Θ but no dependence of the latter on whether the ring is a trefoil- or a 5-fold knot. It merits further investigation to determine the Θ-points of these and more complex knots and examine its dependence on knot complexity but the task is nevertheless demanding, in view of the larger and larger values of N required for more complicated knots. Our findings on ring sizes and the determination of the Θ-point have also been supplemented by an analysis of the shapes and their dependence on topology and solvent conditions. Hereby, we have on the one hand successfully checked the accuracy of our results in comparison with some previously derived ones and on the other we have produced a host of novel results on the asphericity, prolateness, and acylindricity of unknotted and knotted rings under varying solvent quality.

We have also derived the effective potentials $V_{\text{eff}}(R)$ between unknotted rings at worsening solvent quality, finding very significant differences from the ones for their linear counterparts. A calculation of the Boyle temperatures T_B for $N = 100$ ring- and linear-polymers on the basis of these potentials confirms the reduction of T_B for rings as compared to linear chains. For $N = 100$, the knotted polymers considered in this work are too tight for the solvent quality to have large, qualitative effects on their effective potential $V_{\text{eff}}(R)$. Instead, the crowding caused by the (tight) knots dominates the effective interactions. On these grounds, a determination of the Boyle point for knotted rings has not been possible. Simulations with much longer knotted molecules are necessary for this purpose, and they are left as a problem for the future.

APPENDIX

A. Checking Topology

The crank-shaft and pivot moves implemented in the MC- and PHMC-simulations described in section 4 are *not* local and thus they entail the possibility that they result in bond-crossing for the ring polymers, which can result in a spurious (and unwanted) alteration of their topology. To avoid this, we developed an algorithm by which each move is checked for bond-crossing and it is only accepted if the latter does not take place, guaranteeing thereby topology conservation in our simulations. In what follows, we describe the algorithm that checks for bond-crossing for the case in which just one monomer move is attempted. In a pivot algorithm this is, of course, not the case. However, each collective move can be decomposed into successive monomer moves (e.g., in a sequential fashion starting from one pivot point and ending on the other), in which each monomer is moved to a new position, followed by the next. Fig. 12 provides a visualization of the geometry and the parameters explained in the text.

Consider the sequential monomers m, $m + 1$ at positions A_m, A_{m+1}, connected by the bond (A_m, A_{m+1}). Moreover, consider another pair of neighboring, sequential monomers n, $n + 1$, at positions A_n, A_{n+1}, connected by their own bond (A_n, A_{n+1}). Since the algorithm is topology-preserving, the configuration of the bonds is a legitimate one before any attempted move. Thus, to result to another legitimate configuration, we have to exclude the possibility that the move makes the bonds cross through one another.

Suppose we attempt to move monomer $m + 1$ of the polymer from its old position A_{m+1} to a new position A'_{m+1}. Let $l(A_m, A'_{m+1}; t)$ be the line passing through the positions of monomers A_m and A'_{m+1}, parameterized by the oriented length t, which is chosen in such a way that $t = 0$ at the point A_m and $t = 1$ at

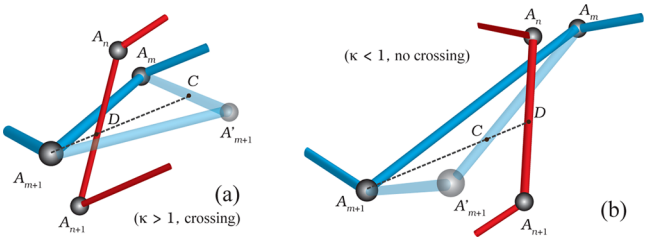

Figure 12. Sketch of the geometry of the neighboring bonds described in the text, showing the pair of connected monomers at positions A_m, A_{m+1} and neighboring pair at positions A_n, A_{n+1}. A'_{m+1} is the attempted new position of monomer $m + 1$. Here we assume that the parameters s_D of point D and t_C of point C (see the text), satisfy the conditions $0 < s_D < 1$ and $0 < t_C < 1$, so that the check on the magnitude of the variable κ, eq 24, has to be carried out. (a) In the case $\kappa > 1$, the new position of the bond (A_m, A'_{m+1}) has crossed the bond (A_n, A_{n+1}) with respect its previous position (A_m, A_{m+1}) before the attempted move of monomer $m + 1$; thus, the move must be rejected. (b) In this case, $\kappa < 1$, and no bond-crossing has taken place.

the point A'_{m+1}. Similarly, let $l(A_n, A_{n+1}; s)$ be the line passing through the positions of monomers A_n and A_{n+1} with the parameter s taking the values $s = 0$ and $s = 1$ at the points A_n and A_{n+1}, respectively. Consider now the old monomer position A_{m+1} as a "point of observation" (in fact, A_{m+1} will be chosen as the origin of the coordinate system later on) and introduce the plane spanned by this point and the line $l(A_m, A'_{m+1}; t)$, which we call $\mathcal{P}(A_{m+1}, A_m, A'_{m+1})$. The steps of the algorithm for checking bond-crossing proceeds now as follows.

1. Find the point $D = \mathcal{P}(A_{m+1}, A_m, A'_{m+1}) \cap l(A_n, A_{n+1}; s)$, i.e., the point of intersection between the plane and the line passing between the points A_n, A_{n+1}. Let s_D be the value of the parameter s for this point.
2. If $s_D < 0$ or $s_D > 1$, there is no crossing between the two bonds, and one proceeds to step 7. If $0 < s_D < 1$, then:
3. Find the point C at which the line passing through A_{m+1} and D intersects the line $l(A_m, A'_{m+1}; t)$. Let t_C be the value of the parameter t for this point.
4. If $t_C < 0$ or $t_C > 1$, there is no crossing between the two bonds, and one proceeds to step 7. If $0 < t_C < 1$, then:
5. Place the origin of the coordinate system at A_{m+1} and let $\mathbf{w}_C$ and $\mathbf{w}_D$ be the collinear position vectors of the points C and D, respectively. Find the value of the variable κ satisfying the equation:

$$\mathbf{w}_C = \kappa \mathbf{w}_D \tag{24}$$

6. If $\kappa < 1$, there is no crossing between the bonds and one proceeds to step 7. (Note that this includes the case $\kappa < 0$). If $\kappa > 1$, bonds have crossed and the move is rejected.
7. Repeat the procedure for other neighboring bonds that could have been crossed though the attempted move. If any of them is crossed, the move is rejected. If not, the usual Metropolis acceptance criterion is employed.

The order of the checks in steps 2, 4, and 6 above is interchangeable; the algorithm has been presented in a way that appears most intuitive but, in practice, the mathematical formulas expressing the three quantities κ, t_C, and s_D lead to an easier way of determining them. We present these expressions below.

Let $\mathbf{P}$ denote the position vector of any point P with respect to some arbitrary origin. Define the vectors

$$\mathbf{u} = \mathbf{A}'_{m+1} - \mathbf{A}_m \tag{25}$$

$$\mathbf{v} = \mathbf{A}_{n+1} - \mathbf{A}_n \tag{26}$$

$$\mathbf{w}_m = \mathbf{A}_m - \mathbf{A}_{m+1} \tag{27}$$

$$\mathbf{w}_n = \mathbf{A}_n - \mathbf{A}_{m+1} \tag{28}$$

The expressions for the sought-for parameters read as follows:

$$\kappa = \frac{\mathbf{w}_m \cdot (\mathbf{u} \times \mathbf{v})}{\mathbf{w}_n \cdot (\mathbf{u} \times \mathbf{v})} \tag{29}$$

$$s_D(\mathbf{u} \times \mathbf{v}) = \mathbf{u} \times (\mathbf{w}_m/\kappa - \mathbf{w}_n) \tag{30}$$

$$t_C \mathbf{u} = \kappa s_D \mathbf{v} + \kappa \mathbf{w}_n - \mathbf{w}_m \tag{31}$$

Thus, one first determines κ from eq 29 and if the inequality $\kappa > 1$ is fulfilled, one proceeds with s_D using eq 30. If $0 < s_D < 1$, t_C is calculated from eq 31 and in case $0 < t_C < 1$ the move is rejected. In all other cases, checks for bond-crossing with other neighboring bonds are performed.

AUTHOR INFORMATION

Corresponding Author

*E-mail: (A.N.) arturo.narros@univie.ac.at.

Notes

The authors declare no competing financial interest.

ACKNOWLEDGMENTS

We acknowledge helpful discussions with Ronald Blaak. The computational results presented have been achieved using the Vienna Scientific Cluster (VSC). The research leading to these results has received funding from the European Community's Seventh Framework Programme (FP7/2007-2013) under the IEF-RINGEFF, Grant Agreement 236664, and by the Austrian Science Fund (FWF), Grant 23400-N16.

REFERENCES

(1) Koniaris, K.; Muthukumar, M. *Phys. Rev. Lett.* **1991**, *66*, 2211−2214.
(2) Neuman, K. C. *J. Biol. Chem.* **2010**, *285*, 18967−18971.
(3) Buck, D. *Proc. Symp. Appl. Math.* **2009**, *66*, 47.
(4) Arsuaga, J.; Vázquez, M.; Trigueros, S.; Sumners, D. W.; Roca, J. *Proc. Natl. Acad. Sci. U.S.A.* **2002**, *99*, 5373−5377.
(5) Champoux, J. J. *Annu. Rev. Biochem.* **2001**, *70*, 369−413.
(6) Wu, F. Y. *Rev. Mod. Phys.* **1992**, *64*, 1099−1131.
(7) Kauffman, L. H. *Knots and Physics*; World Scientific Publishing: Singapore, 1993.
(8) Deguchi, T.; Tsurusaki, K. *Phys. Lett. A* **1993**, *174*, 29−37.
(9) Shimamura, M. K.; Deguchi, T. *Phys. Lett. A* **2000**, *274*, 184−191.
(10) Shimamura, M. K.; Deguchi, T. *Phys. Rev. E* **2002**, *66*, 040801.
(11) Deguchi, T.; Tsurusaki, K. *Phys. Rev. E* **1997**, *55*, 6245−6248.
(12) Marcone, B.; Orlandini, E.; Stella, A. L.; Zonta, F. *Phys. Rev. E* **2007**, *75*, 041105.
(13) Rawdon, E.; Dobay, A.; Kern, J. C.; Millett, K. C.; Piatek, M.; Plunkett, P.; Stasiak, A. *Macromolecules* **2008**, *41*, 4444−4451.
(14) Dobay, A.; Dubochet, J.; Millett, K.; Sottas, P.-E.; Stasiak, A. *Proc. Natl. Acad. Sci. U.S.A.* **2003**, *100*, 5611−5615.
(15) Orlandini, E.; Stella, A. L.; Vanderzande, C. *Phys. Rev. E* **2003**, *68*, 031804.
(16) Orlandini, E.; Whittington, S. G. *Rev. Mod. Phys.* **2007**, *79*, 611−632.
(17) Rosa, A.; Orlandini, E.; Tubiana, L.; Micheletti, C. *Macromolecules* **2011**, *44*, 8668−8680.
(18) Levene, S. D.; Donahue, C.; Boles, T. C.; Cozzarelli, N. R. *Biophys. J.* **1995**, *69*, 1036−1045.

(19) Stasiak, A.; Katritch, V.; Bednar, J.; Michoud, D.; Dubochet, J. *Nature* **1996**, *384*, 122.
(20) Ayme, J.-F.; Beves, J. E.; Leigh, D. A.; McBurney, R. T.; Rissanen, K.; Schultz, D. *Nat. Chem.* **2012**, *4*, 15−20.
(21) McKenna, G. B.; Hadziioannou, G.; Lutz, P.; Hild, G.; Strazielle, C.; Straupe, C.; Rempp, P.; Kovacs, A. J. *Macromolecules* **1987**, *20*, 498−512.
(22) Roovers, J. *Macromolecules* **1985**, *18*, 1359−1361.
(23) Roovers, J. *Macromolecules* **1988**, *21*, 1517−1521.
(24) Hodgson, D. F.; Amis, E. J. *J. Chem. Phys.* **1991**, *95*, 7653−7663.
(25) Robertson, R. M.; Smith, D. E. *Macromolecules* **2007**, *40*, 3373−3377.
(26) Robertson, R. M.; Smith, D. E. *Proc. Natl. Acad. Sci. U.S.A.* **2007**, *104*, 4824−4827.
(27) Takano, A.; Kushida, Y.; Ohta, Y.; Masuoka, K.; Matsushita, Y. *Polymer* **2009**, *50*, 1300−1303.
(28) Steinhauser, M. O. *J. Chem. Phys.* **2005**, *122*, 094901.
(29) Grassberger, P.; Hegger, R. *J. Chem. Phys.* **1995**, *102*, 6881−6899.
(30) Withers, I. M.; Dobrynin, A. V.; Berkowitz, M. L.; Rubinstein, M. *J. Chem. Phys.* **2003**, *118*, 4721−4732.
(31) Krakoviack, V.; Rotenberg, B.; Hansen, J. P. *J. Phys. Chem. B* **2004**, *108*, 6697−6706.
(32) Pelissetto, A.; Hansen, J.-P. *J. Chem. Phys.* **2005**, *122*, 134904.
(33) Dautenhahn, J.; Hall, C. K. *Macromolecules* **1994**, *27*, 5399−5412.
(34) Bohn, M.; Heermann, D. W. *J. Chem. Phys.* **2010**, *132*, 044904.
(35) Iwata, K.; Kimura, T. *J. Chem. Phys.* **1981**, *74*, 2039−2048.
(36) Tanaka, F. *Prog. Theor. Phys.* **1982**, *68*, 148−163.
(37) Tanaka, F. *J. Chem. Phys.* **1987**, *87*, 4201−4206.
(38) Iwata, K. *J. Chem. Phys.* **1983**, *78*, 2778−2787.
(39) Iwata, K. *Macromolecules* **1989**, *22*, 3702−3706.
(40) Vologodskii, A. V.; Lukashin, A. V.; Frank-Kamenetskii, M. D. *Sov. Phys.—JETP.* **1975**, *40*, 932−936.
(41) Marenduzzo, D.; Orlandini, E.; Stasiak, A.; Sumners, De W.; Tubiana, L.; Micheletti, C. *Proc. Nat. Acad. Sci. U.S.A.* **2009**, *106*, 22269−22274.
(42) Marenduzzo, D.; Orlandini, E. *J. Stat. Mech.* **2009**, L09002.
(43) Baiesi, M.; Orlandini, E.; Stella, A. L.; Zonta, F. *Phys. Rev. Lett.* **2011**, *106*, 258301.
(44) Krakoviack, V.; Hansen, J.-P.; Louis, A. A. *Phys. Rev. E* **2003**, *67*, 041801.
(45) Rubinstein, M.; Colby, R. H. *Polymer Physics*; Oxford University Press: New York, 2003.
(46) Bishop, M.; Clarke, J. H. R. *J. Chem. Phys.* **1989**, *90*, 6647−6651.
(47) Batoulis, J.; Kremer, K. *Macromolecules* **1989**, *22*, 4277−4285.
(48) Zifferer, G. *J. Chem. Phys.* **1999**, *110*, 4668−4677.
(49) Theodorou, D. N.; Suter, U. W. *Macromolecules* **1985**, *18*, 1206−1214.
(50) Bishop, M.; Smith, W. *J. Chem. Phys.* **1991**, *95*, 3804−3807.
(51) Cannon, J. W.; Aronovitz, J. A.; Goldbart, P. *J. Phys. I Fr.* **1991**, *1*, 629−645.
(52) Jagodzinski, O.; Eisenriegler, E.; Kremer, K. *J. Phys. I Fr.* **1992**, *2*, 2243−2279.
(53) Zifferer, G.; Preusser, W. *Macromol. Theor. Simul.* **2001**, *10*, 397−407.
(54) Millett, K. C.; Plunkett, P.; Piatek, M.; Rawdon, E. J.; Stasiak, A. *J. Chem. Phys.* **2009**, *130*, 165104.
(55) Rawdon, E. J.; Kern, J. C.; Piatek, M.; Plunkett, P.; Stasiak, A.; Millett, K. C. *Macromolecules* **2008**, *41*, 8281−8287.
(56) Hirayama, N.; Tsurusaki, K.; Deguchi, T. *J. Phys. A: Math. Theor.* **2009**, *42*, 105001.
(57) Narros, A.; Moreno, A. J.; Likos, C. N. *Soft Matter* **2010**, *6*, 2435−2441.
(58) Jang, S. S.; Çağin, T.; Goddard, W. A., III *J. Chem. Phys.* **2003**, *119*, 1843−1854.
(59) Grosberg, A. Y. *Phys. Rev. Lett.* **2000**, *85*, 3858−3861.
(60) Grosberg, A. Y. *arXiv cond-mat* **2002**, 0207427.
(61) Moore, N. T.; Lua, R. C.; Grosberg, A. Y. *Proc. Natl. Acad. Sci. U.S.A.* **2004**, *101*, 13431−13435.
(62) Marcone, B.; Orlandini, E.; Stella, A. L.; Zonta, F. *J. Phys. A* **2005**, *38*, L15−L21.
(63) Bernabei, M.; Bacova, P.; Moreno, A. J.; Narros, A.; Likos, C. N. *Soft Matter* **2013**, *9*, 1287−1300.
(64) Michels, J. P. J.; Wiegel, F. W. *Proc. R. Soc. A Math. Phy.* **1986**, *403*, 269−284.
(65) Grosberg, A. Y.; Feigel, A.; Rabin, Y. *Phys. Rev. E* **1996**, *54*, 6618−6622.
(66) Sun, H.-Q.; Zhang, L.; Liao, Q. *J. Phys. Chem. B* **2010**, *114*, 12293−12297.
(67) Bishop, M.; Michels, J. P. J. *J. Chem. Phys.* **1986**, *85*, 5961−5962.
(68) Huißmann, S.; Blaak, R.; Likos, C. N. *Macromolecules* **2009**, *42*, 2806−2816.
(69) Reddy, G.; Yethiraj, A. *Macromolecules* **2006**, *39*, 8536−8542.
(70) Nasrabad, A. E. *J. Chem. Phys.* **2008**, *128*, 154514.
(71) Accelrys, Inc., Discover 2.9.8/96.0/4.0.0: Forcefields Simulations. 1996.
(72) Grest, G. S.; Kremer, K. *Phys. Rev. A* **1986**, *33*, 3628−3631.
(73) Mehlig, B.; Heermann, D. W.; Forrest, B. M. *Phys. Rev. B* **1992**, *45*, 679−685.
(74) Duane, S.; Kennedy, A. D.; Pendleton, B. J.; Roweth, D. *Phys. Lett. B* **1987**, *195*, 216−222.
(75) Chodera, J. D.; Swope, W. C.; Pitera, J. W.; Seok, C.; Dill, K. A. *J. Chem. Theory Comput.* **2006**, *3*, 26−41.
(76) Escobedo, F. A.; de Pablo, J. J. *J. Chem. Phys.* **1995**, *102*, 2636−2652.
(77) Kumar, S. K.; Vacatello, M.; Yoon, D. Y. *J. Chem. Phys.* **1988**, *89*, 5206−5215.
(78) Todorov, I.; Smith, W. The DL POLY 3 User Manual. STFC Darresbury Laboratory: Daresbury, Warrintor WA4 4AD, Cheshire, U.K., 2008.
(79) Mladek, B. M.; Kahl, G.; Likos, C. N. *Phys. Rev. Lett.* **2008**, *100*, 028301.
(80) Clisby, N.; Liang, R.; Slade, G. *J. Phys. A: Math. Theor.* **2007**, *40*, 10973−11017.
(81) Clisby, N. *Phys. Rev. Lett.* **2010**, *104*, 055702.
(82) Orlandini, E.; Tesi, M. C.; van Rensburg, E. J. J.; Whittington, S. G. *J. Phys. A: Math. Gen.* **1998**, *31*, 5953−5967.
(83) Mansfield, M. L.; Douglas, J. F. *J. Chem. Phys.* **2010**, *133*, 044903.
(84) Krüger, B.; Schäfer, L.; Baumgärtner, A. *J. Phys. (Paris)* **1989**, *50*, 3191−3222.
(85) Narros, A.; Moreno, A. J.; Likos, C. N. *Biochem. Soc. Trans.* **2013**, *41*, 630−634.
(86) Gaspari, G.; Rudnick, J.; Beldjenna, A. *J. Phys. A* **1987**, *20*, 3393−3414.